and co-workers,[14,16] trajectory calculations are needed to determine whether an analogous surface-hopping model for NH($a^1\Delta$) isc can quantatively describe the experimental results.

Acknowledgment. We thank the Office of Naval Research for financial support of this project through the Naval Research Laboratory.

Registry No. NH, 13774-92-0; N_2, 7727-37-9; CO, 630-08-0; Xe, 7440-63-3; O_2, 7782-44-7.

Molecular Reorientation of Nearly Classical Spherical Tops. SeF_6 and TeF_6

Cynthia J. Jameson,*[1a] A. Keith Jameson,*[1b] and Ronald J. Terry[1b]

Departments of Chemistry, University of Illinois at Chicago, Chicago, Illinois 60680, and Loyola University, Chicago, Illinois 60626 *(Received: August 10, 1990; In Final Form: November 9, 1990)*

The cross sections for changes in the rotational angular momentum vector of SeF_6 and TeF_6 upon collisions with Ar, Kr, Xe, N_2, CO, HCl, CO_2, CH_4, CF_4, SF_6, and self have been determined from ^{19}F nuclear spin relaxation measurements in the gas phase. These cross sections are found to have temperature dependences distinctly different from T^{-1}. A general correlation is found between the temperature dependence and the average well depth for a variety of molecules with the same set of collision partners.

Introduction

Rotational relaxation in gases is important for many applications. The relaxation of rotational energy and the relaxation of the rotational angular momentum **J** vector are both of interest. For rotational energy relaxation the best available data are detailed state-to-state rotational energy-transfer cross sections that have been measured by a number of double-resonance laser spectroscopic techniques[2-5] and by microwave transient spectroscopy.[6] Spectra of heavy spherical top molecules such as SF_6, SeF_6, and TeF_6 are generally too congested to permit determination of state-to-state rotational relaxation cross sections, and microwave spectroscopy is not applicable to these molecules. On the other hand, nuclear spin relaxation measurements can provide thermal average cross sections, σ_J, for collisions that cause changes in the **J** vector. These σ_J cross sections are distinct from other rotational relaxation cross sections such as those obtained from IRDR laser experiments, or pressure-broadening, or sound absorption data. Our work in nuclear spin relaxation (T_1) in gases has been motivated by its direct connection and high sensitivity to the anisotropy of the intermolecular potential. The connection is schematically shown as

$$\text{observable} \overset{\text{kinetic theory}}{\leftrightarrow} \text{effective cross section} \overset{\text{scattering theory}}{\leftrightarrow} \text{intermolecular potential}$$

In this context, the effective cross section is a well-defined quantity from both ends. Provided that a single relaxation mechanism (in this case, the spin-rotation mechanism) is responsible for the measured T_1 (or if the T_1 for a particular mechanism can be precisely separated out from the total T_1), provided that experiments are carried out in the intermediate density regime in which T_1 varies linearly with density ρ, then the collision cross sections σ_J, for relaxation of the molecular rotational angular momentum vector **J** has a well-defined relationship to the measured T_1 due to the spin-rotation intramolecular coupling mechanism. For spherical tops this relationship is

$$\left(\frac{T_1}{\rho}\right)_{\text{lin}} = \frac{3}{2C_{\text{eff}}^2\langle J(J+1)\rangle}\bar{v}\sigma_J(T) \qquad (1)$$

C_{eff}^2 is defined in terms of the elements of the spin-rotation tensor. For a spherical top molecule[8]

$$C_{\text{eff}}^2 \equiv [\tfrac{1}{3}(C_\parallel + 2C_\perp)]^2 + \tfrac{4}{45}(C_\parallel - C_\perp)^2 \qquad (2)$$

The assumptions that allow eq 1 to be valid are that (a) the Larmor frequency is small compared to the collision frequency (the "extreme narrowing limit"), (b) the duration of a collision is short compared to the average time between collisions, (c) the interactions among the perturbers do not significantly influence their collisions with the spectroscopic molecule, and (d) bound states between the spectroscopic molecule and the perturber are neglected, all of which are easily satisfied in the linear density regime.

The connection between $\sigma_J(T)$ and the intermolecular potential surface is also well-defined:[9]

$$\sigma_J(T) = [\mathbf{d}\cdot(\sigma)^{-1}\cdot\mathbf{P}\cdot\mathbf{d}]^{-1}$$

where $d_j = \langle J(J+1)\rangle^{-1/2}[J(J+1)]^{1/2}$, and **P** is a diagonal matrix whose elements are proportional to the populations of the J states, normalized such that $\mathbf{d}\cdot\mathbf{P}\cdot\mathbf{d} = 1$. The σ matrix gives the effect of an average collision of a given energy and impact parameter in changing the time development of the **J** vector. The σ matrix elements are defined for the spin-rotation mechanism in ref 9, eq 72, involving elements of the scattering matrix that are averaged over translational initial conditions (energy and impact parameter). In principle, given an intermolecular potential surface, the scattering matrix elements can be calculated, and from these, $\sigma_J(T)$. The problem in applying this theory lies in the difficulty of solving the complex collision dynamics for realistic systems and in obtaining the anisotropic potential surfaces.

We have recently reported the ^{19}F relaxation times in SF_6 molecule in collisions with various molecules.[10] In that work,

(1) (a) University of Illinois at Chicago. (b) Loyola University.
(2) Foy, B.; Hetzler, J.; Millot, G.; Steinfeld, J. I. *J. Chem. Phys.* **1988**, *88*, 6838-6852.
(3) Foy, B.; Laux, L.; Kable, S.; Steinfeld, J. I. *Chem. Phys. Lett.* **1985**, *118*, 464-467.
(4) Taatjes, C. A.; Leone, S. R. *J. Chem. Phys.* **1988**, *89*, 302-308.
(5) Everitt, H. O.; DeLucia, F. C. *J. Chem. Phys.* **1989**, *90*, 3520-3527; **1990**, *92*, 6480-6491.
(6) Odashima, H.; Kajita, M.; Matsuo, Y.; Minowa, T.; Shimizu, T. *J. Chem. Phys.* **1989**, 4875-4878.
(7) Gordon, R. G. *J. Chem. Phys.* **1966**, *45*, 1649-1655.
(8) McCourt, F. R.; Hess, S. *Z. Naturforsch. A* **1971**, *26*, 1234-1236.
(9) Neilsen, W. B.; Gordon, R. G. *J. Chem. Phys.* **1973**, *58*, 4131-4148, 4149-4170.
(10) Jameson, C. J.; Jameson, A. K. *J. Chem. Phys.* **1988**, *88*, 7448-7452.

0022-3654/91/2095-2982$02.50/0

as well as for other probe molecules, the temperature dependence was empirically found to follow the power law $(T_1/\rho) \propto T^{-n}$. The value of n for SF_6 varied from 1.5 to 1.7 depending on collision partner; the largest value for n we have seen in the nearly 100 probe–buffer combinations that we have investigated. Relaxation times have been measured in the gas phase for heavier molecules than SF_6. Examples are T_1 of ^{19}F in MoF_6, WF_6, and UF_6. However, these reported data have been taken in the saturated vapor in equilibrium with the liquid phase.[11] Thus, the observed temperature dependence is due to the temperature dependence of the vapor density as well as the temperature dependence of the relaxation cross sections. Nevertheless, by using empirical vapor pressure data, the authors arrive at $(T_1/\rho) \propto T^{-n}$, where $n = 1.49 \pm 0.04$, 1.51 ± 0.05, and 1.50 ± 0.06 for MoF_6, WF_6, and UF_6, respectively. These are remarkably close to the $T^{-3/2}$ dependence expected from the spin–rotation mechanism in the classical limit. This type of T_1 measurement can be applied only in studies of self-relaxation because the dependence of partial vapor pressures on temperature and composition becomes too difficult to take into account and still find n for ^{19}F relaxation of WF_6 in CO_2, for example. SeF_6 and TeF_6 are molecules that have reasonably high vapor pressures for all-gas measurements over a sizeable temperature range. These probe molecules are heavier than SF_6 and consequently may resolve the question of whether or not $n > 1.5$ for SF_6 is anomalous.

In this paper we report the ^{19}F relaxation times in SeF_6 and TeF_6 in collisions with Ar, Kr, Xe, N_2, CO, HCl, CO_2, CH_4, CF_4, SF_6, and self in all-gas samples. The spin–rotation tensors of ^{19}F in SeF_6 and TeF_6 have previously been determined from the analysis of the rigid-lattice line shapes of SeF_6 and TeF_6 in deuteriohydrates.[12] With the known components of the spin–rotation tensor, it is possible to calculate from $(T_1/\rho)_{SeF_6\text{-}X}$ the cross section $\sigma_J(SeF_6\text{-}X)$ by using Gordon's theory.[7] In eq 1 the thermal average $\langle J(J+1)\rangle$ can be taken as the classical limit $3I_0kT/\hbar^2$, and the mean relative velocity $\bar{v} = (8kT/\pi\mu)^{1/2}$. I_0 is also known from $r(Se\text{–}F) = 1.680$ Å and $r(Te\text{–}F) = 1.811$ Å.[13] These values of σ_J from eq 1 are cross sections for changes in the rotational angular momentum of SeF_6 (or TeF_6) upon collision with an X molecule and are entirely dependent on the anisotropy of the SeF_6–X (or the TeF_6–X) intermolecular potential. As in SF_6–rare gas interactions, the long-range anisotropy in SeF_6–rare gas interactions arises from the permanent hexadecapole moment and the dipole–octopole polarizability as the leading terms. The short-range anisotropy in SF_6–rare gas potentials are found to be surprisingly large.[14,15] With the longer Se–F and Te–F bonds, the short-range anisotropy in the SeF_6 (or TeF_6)–rare gas potential would be large too. Indeed we find in this study that the efficiency of collisions with various molecules in changing the rotational angular momentum of SeF_6 and TeF_6 are greater than the corresponding ones for SF_6.

Experimental Section

The experimental procedure is as described earlier.[10] Sealed samples of pure SeF_6 (4–30 amagat), pure TeF_6 (3–25 amagat), and 1.5–2 amagat of SeF_6 or TeF_6 in 10–35 amagat of buffer gas (Ar, Kr, Xe, N_2, CO, HCl, CO_2, CH_4, CF_4, SF_6) were prepared by freezing out each gas into the precalibrated sample tube from a calibrated section of the vacuum line. ^{19}F NMR relaxation time measurements in SeF_6 and TeF_6 molecules in these samples were carried out by the inversion recovery method primarily on a Bruker WP80 (operating at 1.9 T) and some on an IBM WP200SY (at 4.7 T). Relaxation times obtained with the two spectrometers were virtually identical. The internal shift of ethylene glycol was used for temperature determination above room temperature and

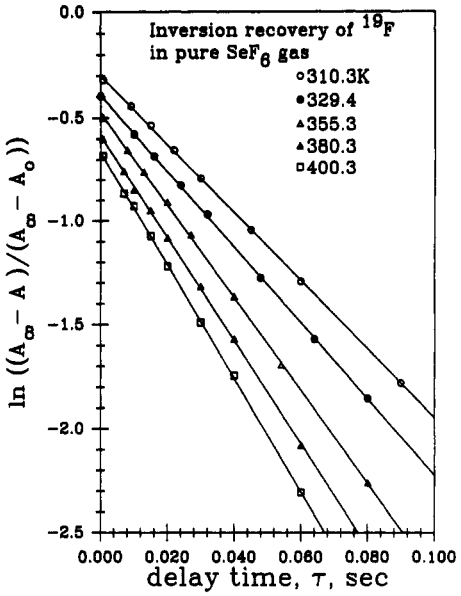

Figure 1. Typical inversion recovery data for ^{19}F in SeF_6. This example is for SeF_6 in 20 amagat of pure SeF_6 gas. The ordinate of each line has been displaced for display purposes. The slope of each line is $-1/T_1$.

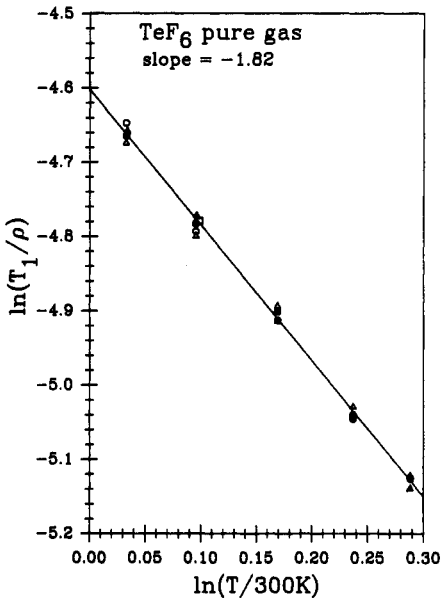

Figure 2. Power law dependence of T_1 on temperature for TeF_6 molecule in pure TeF_6 gas. The power in this case is −1.82.

methanol below room temperature. The temperature range of this study (295–400 K) was limited by condensation of SeF_6 or TeF_6 at the low end of the range. The density of vapor in equilibrium with the liquid at 290 K is 14.0 amagat for SeF_6 and 9.5 amagat for TeF_6.[16] Thus, to have a sizeable range of densities ρ over which to determine (T_1/ρ) in all-gas samples of the pure compounds, we limited our studies to 295–400 K. Not all the samples of pure SeF_6 and TeF_6 remained all gas below 310 K, so we report (T_1/ρ) for pure SeF_6 and TeF_6 only for the range 310–400 K. Samples with 1–2 amagat of SeF_6 or TeF_6 in the buffer gases would of course remain all gas to much lower temperatures. However, since we have not characterized the SeF_6–SeF_6 or TeF_6–TeF_6 contributions to relaxation at these lower temperatures, we cannot extrapolate their temperature dependence to those temperatures. Thus, we report (T_1/ρ) for SeF_6–buffer and TeF_6–buffer in the temperature range 295–400 K. Further experimental details are given in ref 17. T_1 experiments with

(11) Ursu, I.; Bogdan, M.; Fitori, P.; Darabont, A.; Demco, D. E. *Mol. Phys.* **1985**, *56*, 297–302.
(12) Garg, S. K.; Ripmeester, J. A.; Davidson, D. W. *J. Magn. Reson.* **1980**, *39*, 317–323.
(13) Stanton, J. F.; Bartell, L. S. *J. Phys. Chem.* **1985**, *89*, 2544–2549.
(14) Pack, R. T.; Valentini, J. J.; Cross, J. B. *J. Chem. Phys.* **1982**, *77*, 5486–5499.
(15) Pack, R. T.; Piper, F.; Pfeffer, G. A.; Toennies, J. P. *J. Chem. Phys.* **1984**, *80*, 4940–4950.
(16) Oppusunggu, D. H. Ph.D. Thesis, University of Illinois at Chicago, 1989.
(17) Terry, R. J. Ph.D. Thesis, Loyola University, 1989.

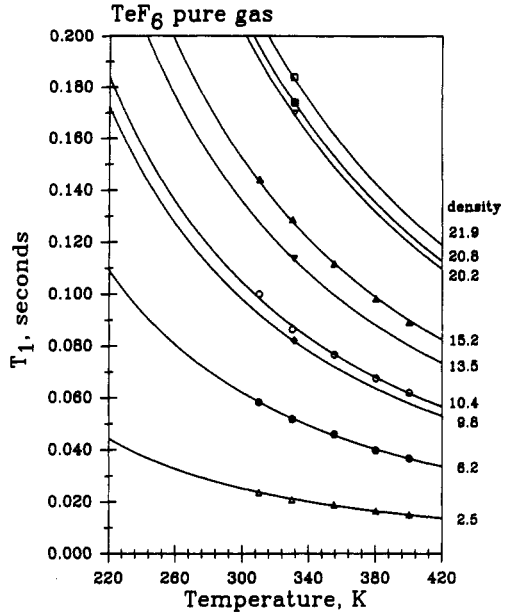

Figure 3. Temperature dependence of T_1 for various samples of pure TeF_6. The densities (in amagat) are shown. All the curves are generated from the $(T_1/\rho)_{300K}$ and power −1.82 found in Figure 2.

TABLE I: Spin Relaxation Times for ^{19}F in SeF_6 in Various Buffer Gases. The Observed Temperature Dependence Is Described by

$$(T_1/\rho)_T = (T_1/\rho)_{300K}(T/300)^n$$

buffer	$(T_1/\rho)_{300K}$, ms amagat^{-1}	n	T range, K
CH_4	0.96 ± 0.02	−1.82 ± 0.07	295–400
N_2	0.87 ± 0.01	−1.74 ± 0.05	295–400
CO	0.97 ± 0.03	−1.76 ± 0.08	295–400
Ar	1.00 ± 0.04	−1.69 ± 0.11	295–400
HCl	1.32 ± 0.05	−1.74 ± 0.09	295–400
CO_2	1.67 ± 0.04	−1.84 ± 0.06	295–400
Kr	1.52 ± 0.04	−1.89 ± 0.07	295–400
CF_4	2.16 ± 0.05	−1.98 ± 0.06	295–400
Xe	1.70 ± 0.04	−1.96 ± 0.08	295–400
SF_6	2.69 ± 0.09	−1.91 ± 0.09	310–400
SeF_6	3.21 ± 0.07	−1.97 ± 0.05	310–400

better than 1% standard deviation in the determination of T_1 were considered acceptable. Relaxation times range from 0.005 to 0.11 s for SeF_6 depending on buffer gas, density, and temperature, while relaxation times range from 0.016 to 0.35 s for TeF_6 in buffer gases.

Results

Typical results are shown in Figures 1 and 2. From the log–log plot of (T_1/ρ) vs T, one obtains the best fit to $(T_1/\rho)_{300K}$ and n in

$$T_1/\rho = (T_1/\rho)_{300K}(T/300)^n \quad (3)$$

It is evident from Figure 2 that this is an adequate description of the temperature dependence. The two parameters $(T_1/\rho)_{300K}$ and n are then used to generate all the curves in Figure 3, which gives an indication of how closely the T_1 data are described by a linear dependence on density and a power law dependence on temperature. For SeF_6 molecule in buffer gas X

$$T_1 = (T_1/\rho)_{SeF_6\text{-}SeF_6}\rho_{SeF_6} + (T_1/\rho)_{SeF_6\text{-}X}\rho_X \quad (4)$$

in which $(T_1/\rho)_{SeF_6\text{-}X}$ is also found to have the form given in eq 3. Straight lines of the type shown in Figure 2 are obtained in each of the 22 cases studied here. Plots of the type shown in Figure 3 are routinely generated to check consistency of the fits with experimental data and for systematic errors. Summaries of these results are given in Tables I and II for SeF_6–X and TeF_6–X. Uncertainties quoted are 1 standard deviation.

TABLE II: Spin Relaxation Times for ^{19}F in TeF_6 in Various Buffer Gases. The Observed Temperature Dependence Is Described by

$$(T_1/\rho)_T = (T_1/\rho)_{300K}(T/300)^n$$

buffer	$(T_1/\rho)_{300K}$, ms amagat^{-1}	n	T range, K
CH_4	3.89 ± 0.09	−2.01 ± 0.07	295–400
N_2	2.78 ± 0.08	−1.78 ± 0.07	295–400
CO	3.92 ± 0.08	−1.87 ± 0.08	295–400
Ar	4.03 ± 0.06	−1.84 ± 0.05	295–400
HCl	4.95 ± 0.21	−1.90 ± 0.14	295–400
CO_2	6.07 ± 0.18	−2.11 ± 0.09	295–400
Kr	5.16 ± 0.13	−1.87 ± 0.08	295–400
CF_4	7.10 ± 0.10	−1.83 ± 0.04	295–400
Xe	5.96 ± 0.10	−2.03 ± 0.04	295–400
SF_6	9.83 ± 0.26	−2.12 ± 0.08	310–400
TeF_6	10.03 ± 0.10	−1.82 ± 0.02	310–400

TABLE III: Relaxation Cross Sections for the Rotational Angular Momentum Vector in SeF_6 with Various Collision Partners. The Observed Temperature Dependence Can Be Described by

$$\sigma_J(T) = \sigma_J(300\text{ K})(T/300)^m$$

collision partner	σ_J(300 K),[a] Å^2	m	r_0,[b] Å	σ_{geom}, Å^2	σ_J/σ_{geom}[c]
CH_4	12.32 ± 0.36	−1.32 ± 0.07	4.685	68.95	0.18
N_2	14.38 ± 0.27	−1.24 ± 0.05	4.468	62.72	0.24
CO	16.04 ± 0.57	−1.26 ± 0.08	4.546	64.92	0.25
Ar	19.37 ± 0.86	−1.19 ± 0.11	4.375	60.13	0.32
HCl	24.54 ± 0.87	−1.24 ± 0.09	4.419	61.35	0.40
CO_2	33.54 ± 0.82	−1.34 ± 0.06	4.550	65.04	0.51
Kr	38.9 ± 1.1	−1.39 ± 0.07	4.514	64.01	0.61
CF_4	56.2 ± 1.4	−1.48 ± 0.06	4.965	77.44	0.73
Xe	50.4 ± 1.3	−1.46 ± 0.08	4.708	69.63	0.72
SF_6	82.2 ± 2.6	−1.41 ± 0.09	5.376	90.80	0.91
SeF_6	105.2 ± 2.2	−1.47 ± 0.05	5.50	95.03	1.11

[a] Quoted error reflects only the standard deviation of (T_1/ρ), not including the uncertainties in the magnitude of the spin-rotation constant for ^{19}F in SeF_6 molecule. [b] These r_0 values are r_0 for SF_6 with the respective collision partners augmented by 0.124 Å, where 0.124 Å is the difference between the SeF_6 and SF_6 bond lengths. [c] Collision efficiencies at 300 K.

TABLE IV: Relaxation Cross Sections for the Rotational Angular Momentum Vector in TeF_6 with Various Collision Partners. The Observed Temperature Dependence Can Be Described by

$$\sigma_J(T) = \sigma_J(300\text{ K})(T/300)^m$$

collision partner	σ_J(300 K),[a] Å^2	m	r_0,[b] Å	σ_{geom}, Å^2	σ_J/σ_{geom}[c]
CH_4	17.68 ± 0.41	−1.51 ± 0.07	4.816	72.87	0.24
N_2	16.41 ± 0.48	−1.28 ± 0.07	4.600	66.48	0.25
CO	18.70 ± 0.46	−1.37 ± 0.08	4.677	68.72	0.27
Ar	27.66 ± 0.46	−1.34 ± 0.05	4.506	63.79	0.43
HCl	32.7 ± 1.3	−1.40 ± 0.14	4.550	65.04	0.50
CO_2	43.3 ± 1.2	−1.61 ± 0.09	4.681	68.84	0.63
Kr	47.7 ± 1.2	−1.37 ± 0.08	4.645	67.78	0.70
CF_4	66.2 ± 1.3	−1.21 ± 0.06	5.096	81.58	0.81
Xe	64.6 ± 1.2	−1.53 ± 0.04	4.839	73.56	0.88
SF_6	109.6 ± 2.8	−1.62 ± 0.08	5.507	95.28	1.15
TeF_6	129.0 ± 1.2	−1.32 ± 0.02	5.762	104.30	1.24

[a] Quoted error reflects only the standard deviation of (T_1/ρ), not including the uncertainties in the magnitude of the spin-rotation constant for ^{19}F in TeF_6 molecule. [b] These r_0 values are r_0 for SF_6 with the respective collision partners augmented by 0.255 Å, where 0.255 Å is the difference between the TeF_6 and SF_6 bond lengths. [c] Collision efficiencies at 300 K.

The temperature dependence is reasonably well characterized despite the limited temperature range. One of the puzzling results in our earlier work on SF_6 relaxation in various buffer gases was the steeper temperature dependence of T_1 in SF_6 (compared to other systems such as CF_4), i.e., $T_1 \sim T^{-n}$ where $n > {}^3/_2$ for SF_6 in most of the buffer gases studied. This appeared to be an unusual

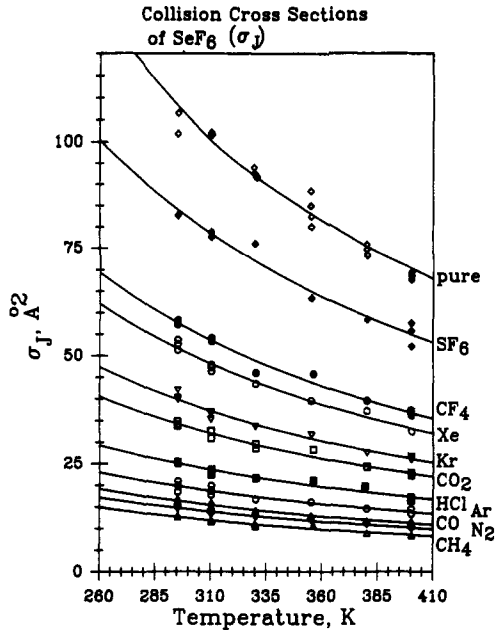

Figure 4. Cross sections $\sigma_J(T)$ for SeF_6 with various collision partners. The curves are derived from power-law fits to temperature of (T_1/ρ) data.

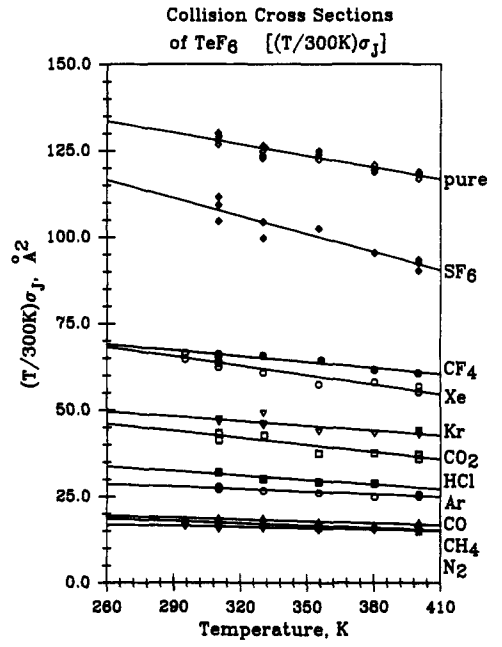

Figure 5. Cross sections $\sigma_J(T)$ multiplied by $(T/300)$ for TeF_6 with various collision partners. These values being temperature-dependent indicates that the $\sigma_J(T)$ have behavior significantly different from T^{-1}.

behavior. Nearly all other systems we have studied, CH_4 (^{13}C or ^1H),[18] ^{19}F in CF_4,[19] ^{15}N in N_2[20] and NNO,[21] and ^{13}C in CO_2[22] and CO,[23] have $n \lesssim {}^3/_2$ in the same set of buffers. Therefore, SeF_6 and TeF_6 are logical probe molecules to determine whether SF_6 is unique in this respect. As the results in Tables I and II show, n is greater than $^3/_2$ in all cases, which offers some reassurance that the SF_6 results were not in error.

TABLE V: Comparison of Our Results with Those of Ref 11 for Hexafluorides:

$$\sigma_J(T) = \sigma_J(300\text{ K})(T/300)^m$$

Z		σ_J(300 K)	σ_{geom}	σ_J/σ_{geom}	m
16	SF_6–SF_6	64.1	86.66	0.74	−1.25 ± 0.02
34	SeF_6–SeF_6	105.2	95.03	1.11	−1.47 ± 0.05
52	TeF_6–TeF_6	129.0	104.30	1.26	−1.32 ± 0.02
42	MoF_6–MoF_6	36.6[a]	77.25[b]	0.47	−0.99 ± 0.04
74	WF_6–WF_6	56.9[a]	83.28[b]	0.68	−1.01 ± 0.05
92	UF_6–UF_6	63.7[a]	86.22[b]	0.74	−1.00 ± 0.06

[a] From ref 11, extrapolated to 300 K based on their Figure 2. [b] Reference 11.

The cross sections σ_J for changes in the rotational angular momentum vector are calculated by using eq 1, and these are shown in Tables III and IV. Typical temperature-dependent cross sections in this study are shown for SeF_6 in Figure 4. The cross sections for TeF_6 are plotted as $(T/300)\sigma_J(T)$ in Figure 5 to illustrate that the temperature dependence of $\sigma_J(T)$ is significantly different from T^{-1}. The latter behavior would give only horizontal lines in this type of plot.

Discussion

Comparisons of the efficiencies of various collision partners in changing the rotational angular momentum of the SeF_6 or TeF_6 molecule can be made if some reasonable scaling can be carried out that takes into account the molecular sizes. Usually we have used the r_0 in the potential function determined by fitting thermophysical properties to collision integrals that are universal functions, chosen such that the intermolecular potentials are rendered conformal by the choice of the two scaling factors ϵ and r_0 for various molecular pairs. Table A3.2 from Maitland et al.[24] provides such values for SF_6 with various collision partners. Unfortunately, similar information is not available for SeF_6 or TeF_6 with any of the collision partners used here since there is essentially no information on the thermophysical properties of pure SeF_6 or TeF_6 or any of their mixtures with other gases. Therefore, we adopt an $r_0(SeF_6\text{–}X)$ from $r_0(SF_6\text{–}X)$ modified by the difference in Se–F and S–F bond lengths, i.e., 1.680 − 1.5561[25] = 0.124 Å is added to all $r_0(SF_6\text{–}X)$ to obtain $r_0(SeF_6\text{–}X)$. A similar approach is taken for TeF_6, i.e., 1.811 − 1.5561 = 0.255 Å is added to all $r_0(SF_6\text{–}X)$ to obtain $r_0(TeF_6\text{–}X)$. This procedure largely accounts for differences in the repulsive parts of the SF_6–X and SeF_6–X potentials, but $\sigma_{geom} = \pi r_0^2$ is somewhat inconsistent with other σ_{geom} that we have used in that the differences in the attractive parts of the SF_6–X and SeF_6–X interactions are not taken into account. Thus, the procedure leads to perhaps a slightly larger $r_0(TeF_6\text{–}X)$ than might be appropriate. Nevertheless we adopt this procedure as the only reasonable way of arriving at an internally consistent set of values of σ_{geom}. We show these results in Tables III and IV. The buffer gases are arranged in order of increasing mass (or number of electrons). We find the σ_J/σ_{geom} monotonically increasing in this order, which may be taken in support of the method of determining σ_{geom}.

A comparison of our work with the results reported for other spherical tops WF_6, MoF_6, and UF_6[11] is shown in Table V. It appears that the general trends in their results are not consistent with ours. Their values of σ_J for MoF_6–MoF_6, WF_6–WF_6, and

(18) Jameson, C. J.; Jameson, A. K.; Smith, N. C.; Hwang, J. K.; Zia, T. *J. Phys. Chem.* **1991**, *95*, 1092–1098.
(19) Jameson, C. J.; Jameson, A. K. *J. Chem. Phys.* **1988**, *89*, 866–870.
(20) Jameson, C. J.; Jameson, A. K.; Smith, N. C. *J. Chem. Phys.* **1987**, *86*, 6833–6838.
(21) Jameson, C. J.; Jameson, A. K.; Hwang, J. K.; Smith, N. C. *J. Chem. Phys.* **1988**, *89*, 5642–5649.
(22) Jameson, C. J.; Jameson, A. K.; Smith, N. C.; Jackowski, K. *J. Chem. Phys.* **1987**, *86*, 2717–2722.
(23) Jameson, C. J.; Jameson, A. K.; Buchi, K. *J. Chem. Phys.* **1986**, *85*, 697–700.
(24) Maitland, G. C.; Rigby, M.; Smith, E. B.; Wakeham, W. A. *Intermolecular Forces, Their Origin and Determination*; Clarendon Press: Oxford, 1981.
(25) Krohn, B. J.; Overend, J. *J. Phys. Chem.* **1984**, *88*, 564–574.
(26) Seip, H. M.; Seip, R. *Acta Chem. Scand.* **1966**, *20*, 2698.
(27) Kimura, M.; Schomaker, V.; Smith, D. W.; Weinstock, B. *J. Chem. Phys.* **1968**, *48*, 4001.
(28) Aldridge, J. P.; Brock, E. G.; Filip, H.; Flicker, H.; Fox, K.; Galbraith, H. W.; Holland, R. F.; Kim, K. C.; Krohn, B. J.; Magnuson, D. W.; Maier, W. B.; McDowell, R. S.; Patterson, C. W.; Person, W. B.; Smith, D. F.; Werner, G. K. *J. Chem. Phys.* **1985**, *83*, 34–48.
(29) Seppelt, K.; Bartlett, N. *Z. Anorg. Allg. Chem.* **1977**, *436*, 122–126.
(30) Jameson, C. J.; Jameson, A. K.; Burrell, P. M. *J. Chem. Phys.* **1980**, *73*, 6013–6020.

TABLE VI: Parameters Used in Calculation of Cross Sections for MoF_6, WF_6, and UF_6, Compared with SeF_6 (References Given in Square Brackets)

property	SeF_6	MoF_6	WF_6	UF_6
bond length/Å	1.680 [13]	1.8203 [26]	1.8318 [27]	1.9962 [28]
$B_0/10^6$ kHz	2.3563	2.0526	1.9945	1.6726
$\delta(^{19}F)$/ppm				764 [29]
absolute σ/ppm, this work	140 [12]	-84.0	33.5	-575[a]
C_{av}/kHz, this work	-4.46	-6.52	-4.99	-10.0
ΔC/kHz	4.47 [12]			
C_{eff}/kHz, this work[b]	4.655	6.80	5.21	10.46
C_{eff}/kHz		3.26 [11]	3.10 [11]	5.84 [11]
σ_{geom}/Å^2, this work[c]	95	105	106	118
σ_{geom}/Å^2		77.25 [11]	83.28 [11]	86.22 [11]
$(T_1/\rho)_{300K}$/ms amagat^{-1}[d]		1.92	2.65	0.65
σ_J(300 K)/Å^2, this work[e]	105.2	162	161	205
σ_J/σ_{geom}	1.11	1.5	1.5	1.7

[a] Absolute shielding ≈ 188.7 ppm - $\delta(^{19}F)$.[30] No correction has been made for the intermolecular effects, which could be a few ppm in a solution of UF_6 in $CFCl_3$. [b] Assuming $\Delta C \approx |C_{av}|$ in eq 2 where C_{av} is taken from the values in this work. [c] Using our method for estimating σ_{geom}, as described in the text, from the $r_0(SF_6\text{–}SF_6)$ and the difference in bond lengths between S–F and Mo–F, or U–F bonds. These values of σ_{geom} are probably overestimated, the greater polarizability of these hexafluorides compared to SF_6 should make r_0 shorter for MoF_6–MoF_6, etc., than the values estimated here. [d] Estimated from extrapolation of the curves in the Figure 2 of ref 11 to 300 K. [e] Calculated from the C_{eff} estimated in this work and the $(T_1/\sigma)_{300K}$ values in this table.

UF_6–UF_6 are much smaller than the ones we have found for SeF_6 and TeF_6. Their estimates for σ_{geom} are likewise smaller than one would have found using the method of estimation described here. Finally, their temperature dependence for σ_J is T^{-1} in every case, whereas ours is not.

There are several difficulties associated with their measurements. T_1 was measured in the vapor in equilibrium with liquid. The vapor density being strongly temperature-dependent, the observed T_1 in the vapor increased with increasing temperature, in contrast to our Figure 3. The use of vapor density functions from the literature thus makes the determination of the temperature dependence of (T_1/ρ) less direct than in a constant-density all-gas sample. A more serious drawback is the lack of an independent measure of the ^{19}F spin rotation tensor in MoF_6, WF_6, and UF_6 molecules. In ref 11, $C_{av} = {}^1/_3(C_\parallel + 2C_\perp)$ was estimated from the values of the ^{19}F chemical shifts obtained from high-resolution NMR spectra and $\Delta C = C_\parallel - C_\perp$ was estimated from the T_1 measurements in the solid state. Using this method, we obtain values of C_{av} that are significantly different from theirs, however. The parameters we used are shown in Table VI with SeF_6 for comparison. We use the identity that relates the components of the nuclear magnetic shielding tensor (unfortunately, the latter is also represented by σ) and the spin–rotation tensor:

$$\sigma_{av}^{SR} = \frac{C_{av}}{B_0}\frac{m_p}{2m_e g(^{19}F)} \quad (5)$$

and the rather good approximation

$$\sigma_{av} = \sigma(\text{free F atom}) + \sigma_{av}^{SR} \quad (6)$$

where the g value of ^{19}F nucleus is 5.257 72[31] and σ(free F atom) = 470.71 ppm.[32] The value of C_{av} we obtained for SeF_6 is of course the same as given by Garg et al.[12] since we use the same Se–F bond length and the same ^{19}F absolute shielding σ_{av} for SeF_6 as Garg et al. reported. We find for MoF_6, WF_6, and UF_6 much larger values of C_{av} than the values of C_{eff} estimated by ref 11, leading to much larger σ_J cross sections than they report. Since intermolecular effects are generally deshielding, having used liquid-phase values for $\delta(^{19}F)$ in MoF_6, WF_6, and UF_6 would lead to $|C_{av}|$ that are somewhat too large and thus cross sections slightly too large. To have arrived at their too small values of C_{eff}, however, ref 11 must have used an incorrect procedure. For a more accurate determination of C_{av} for ^{19}F in MoF_6 and WF_6 we determined the absolute shielding of ^{19}F in the vapor (in equilibrium with the liquid phase) at 300 K. These were obtained by measuring the differences between $\sigma(MoF_6$ vapor, 300 K), $\sigma(WF_6$ vapor, 300 K) and $\sigma(SiF_4$ gas, ρ = 26.24 amagat, 300 K). The absolute shielding of ^{19}F in SiF_4 is 363.2 ppm, known from our previous work.[30] The SiF_4 shielding in the gas sample was corrected (-0.508 ppm) for intermolecular effects based on our earlier work. The WF_6 shielding was also corrected for intermolecular effects by using data previously obtained in our laboratory, reported in ref 16. The latter correction is -0.044 ppm. The correction for MoF_6 is even smaller since its vapor density at 300 K is less than half that of WF_6. Our results based on $\sigma_0(^{19}F, SiF_4, 300\ K) = 363.2$ ppm are

$$\sigma_0(^{19}F, MoF_6, 300\ K) = -84.0 \text{ ppm}$$

$$\sigma_0(^{19}F, WF_6, 300\ K) = +33.5 \text{ ppm}$$

From these absolute shieldings in the zero-pressure limit, we calculated C_{av} using eqs 5 and 6. With our values of C_{av} for MoF_6, WF_6, and UF_6, we find that the values of self cross sections for these molecules at 300 K shown in Table VI form a more consistent trend with the values found for SF_6, SeF_6, and TeF_6 than do the cross sections reported in ref 11 and shown in Table V.

The comparison of ^{19}F relaxation in the related molecules, SF_6, SeF_6, TeF_6, in collisions with the set of 10 collision partners plus self is also interesting. For a given collision partner there is a clear trend across the series SF_6, SeF_6, TeF_6 that is evident in Table VII. Some of the σ_J trend is due to size, which has been removed in the σ_J/σ_{geom} comparison. The latter may be considered as a collision efficiency and is seen to increase monotonically across the series SF_6, SeF_6, TeF_6 for all collision partners. Most of the efficiencies found here are less than 1.0, except for SeF_6 in SF_6, SeF_6–SeF_6, and TeF_6–TeF_6. With the trends shown here, one could predict that the collision efficiency for SeF_6 in TeF_6 and for TeF_6 in SeF_6 would also be greater than 1.0. For a given collision partner, the monotonic increase in collision efficiency across the series SF_6, SeF_6, TeF_6 parallels the expected variation in the well depth of the isotropic part of the intermolecular potential. The polarizabilities of SF_6, SeF_6, and TeF_6 molecules are 6.505×10^{-24}, 7.73×10^{-24}, and 9.00×10^{-24} cm^{-3}, respectively.[33] The second virial coefficient of nuclear magnetic shielding for SF_6–SF_6, SeF_6–SeF_6, and TeF_6–TeF_6 interactions are -0.0156, -0.0316, and -0.0365 ppm amagat^{-1} at 300 K.[34] These properties

TABLE VII: Cross Sections for Angular Momentum Transfer, σ_J, for ^{19}F in SF_6, SeF_6, and TeF_6 with Various Collision Partners at 300 K

collision partner	σ_J, Å^2			σ_J/σ_{geom}		
	SF_6	SeF_6	TeF_6	SF_6	SeF_6	TeF_6
CH_4	9.1	12.3	17.7	0.14	0.18	0.24
N_2	11.0	14.4	16.4	0.19	0.23	0.25
CO	12.0	16.0	18.7	0.19	0.25	0.27
Ar	16.1	19.4	27.7	0.28	0.32	0.43
HCl	16.1	24.5	32.7	0.28	0.40	0.50
CO_2	25.0	33.5	43.3	0.41	0.52	0.63
Kr	27.0	38.9	47.7	0.45	0.61	0.70
CF_4	39.6	56.2	66.2	0.54	0.72	0.82
Xe	34.8	50.4	64.6	0.53	0.72	0.88
SF_6	64.1	82.2	109.6	0.74	0.91	1.15
SeF_6	105.2				1.11	
TeF_6			129.1			1.26

(31) Lederer, C. M.; Shirley, V. S. *Table of Isotopes*, 7th ed.; Wiley: New York, 1978; Appendix VII.
(32) Malli, G.; Froese, C. *Int. J. Quantum. Chem.* **1967**, *S1*, 95–98.
(33) Landolt-Börnstein, *Zahlenwerte und Funktionen*; Springer-Verlag: Berlin, 1962; Vol. II, p 8.
(34) Jameson, C. J.; Jameson, A. K.; Oppusunggu, D. *J. Chem. Phys.* **1986**, *85*, 5480–5483.

TABLE VIII: Temperature Dependence of Cross Sections σ_J for SF_6, SeF_6, and TeF_6 in Collision with Various Molecules. Values of m Are Given for $\sigma_J(T) = \sigma_J(300\ K)(T/300)^m$, Compared with CF_4

collision partner	CF_4	SF_6	SeF_6	TeF_6
CH_4	−0.95	−0.99	−1.32	−1.51
N_2	−0.77	−1.07	−1.24	−1.28
CO	−0.74	−1.07	−1.26	−1.37
Ar	−0.51	−0.97	−1.19	−1.34
HCl	−0.88	−0.94	−1.24	−1.40
CO_2	−1.06	−1.16	−1.34	−1.61
Kr	−0.93	−1.12	−1.39	−1.37
CF_4	−0.91	−1.21	−1.48	−1.33
Xe	−0.97	−1.23	−1.46	−1.53
SF_6	−0.92	−1.25	−1.41	−1.62
SeF_6			−1.47	
TeF_6				−1.32

are intimately linked to the intermolecular potential. However, since other molecular properties parallel this change it may not be a significant correlation.

General Trends in the Temperature Dependence of the Cross Sections σ_J. We have measured a sufficiently large number of cross sections σ_J to find interesting general trends in the magnitudes at room temperature, which we have reported elsewhere.[36] With the present study, we have also measured a sufficiently large number of temperature dependences of the cross sections to note general trends in the temperature dependence.

In the high translational energy limit, the cross section σ_J is expected to have a temperature dependence that is T^{-1}.[35] In this study the temperature dependences of the cross sections of SeF_6 and TeF_6 are uniformly found to be different from T^{-1}. Also interesting is the comparison of the temperature dependences of these cross sections in the series SF_6, SeF_6, TeF_6, shown in Table VIII and compared with the corresponding values for CF_4. There is a monotonic increase in $|m|$ in

$$\sigma_J(T) = \sigma_J(300\ K)(T/300)^m$$

with few exceptions (only three) in going across the series CF_4, SF_6, SeF_6, TeF_6.

It has been previously stated that the temperature variation of T_1/ρ gives little independent information about the anisotropic potential beyond the increase in precision from repeated trials, at least in the case of HCl–Ar because all anisotropic potentials gave the same linear temperature dependence of the log of T_1/ρ on the log of temperature with nearly the same slope, $-3/2$.[9] Indeed, the early reports of spin–rotation relaxation in the gas phase gave such a slope within experimental errors, implying that the cross section σ_J itself has a universal T^{-1} dependence, just as predicted by the model of Johnson and Waugh,[35] in the limiting case of a classical duration of a collision being related to the ratio of a molecular dimension to the relative velocity of the colliding pair. For the other molecules we have studied (CH_4, CO, CO_2, N_2, NNO, CF_4), the observed temperature dependence of $\sigma_J(T)$ is indeed close to T^{-1} in many instances, and many examples of $|m| < 1.0$ were found.[18-23] Deviations from this behavior, first observed for SF_6, were surprising.[10] It is now clear in Table VIII that SF_6 is only the first of many examples where the temperature dependence of the collision cross section differs markedly from the high-temperature classical limit and $|m| > 1.0$. It is not yet known what $|m| > 1.0$ or $|m| < 1.0$ implies for cross sections of a given molecule. We have found $|m|$ significantly less than 1.0 in N_2 molecule. That SF_6, SeF_6, and TeF_6 uniformly have $|m| > 1.0$ for all collision partners suggests a general characteristic of either the target molecule itself or the nature of collisions that are most effective in contributing to σ_J. In Table IX we compare

TABLE IX: Temperature Dependence of σ_J for Various Molecules: $\sigma_J(T) = \sigma_J(300\ K)(T/300)^m$

molecule	average m[a]	range of m values	ref	av ϵ/k, K[b]
N_2	−0.77	−0.60 ± −0.98	20	142
CO	−0.78	−0.61 ± −0.95	23	146
CF_4	−0.90	−0.74 ± −1.06	19	171
CH_4	−0.91	−0.79 ± −1.11	18	180
NNO	−0.92	−0.81 ± −1.04	21	230
CO_2	−0.94	−0.74 ± −1.10	22	212
SF_6	−1.10	−0.94 ± −1.25	10	201
SeF_6	−1.34	−1.19 ± −1.48	this work	243[c]
TeF_6	−1.43	−1.28 to −1.62	this work	287[c]

[a] The average has been taken over the m values of 8–11 collision partners from the set CH_4, N_2, CO, Ar, HCl, CO_2, NNO, Kr, CF_4, C_2H_6, Xe, SF_6, SeF_6, TeF_6. [b] The average has been taken over the ϵ/k values of the intermolecular potential of these molecules interacting with the same set of 12 collision partners as for footnote *a*, except that SeF_6 and TeF_6 were excluded. Values of ϵ/k were taken primarily from the energy scaling parameters given in Maitland et al.,[24] Table A3.1, and also in ref 37 (for CO–CO), ref 38 (for HCl–HCl), ref 39 (for NNO–NNO, NNO–N_2, NNO–CO_2, and NNO–Ar). The rest were obtained by using a geometric mean. [c] The values of ϵ/k for SeF_6–X and TeF_6–X collision pairs were estimated by the method discussed in the text; X = SeF_6, TeF_6 were included.

the value of m averaged over 8–11 of the set of collision partners used here, for each of the target molecules whose σ_J cross sections we have studied as a function of temperature. The rank order according to the average value of $|m|$ is

$$N_2 \approx CO < CF_4 \lesssim CH_4 \lesssim NNO \lesssim CO_2 < SF_6 < SeF_6 < TeF_6$$

There is a rough correspondence with the average well-depth parameter, except for NNO and CO_2 being low. Likewise, the rank order of collision partners according to the average value of $|m|$ is

$$Ar < N_2 \approx CO < Kr < CF_4 < HCl < CH_4 < Xe < CO_2 < SF_6$$

which order is also in rough correspondence with the average well-depth parameter, except that HCl and CO_2 are low, as is the Ar, Kr, Xe series. In a closer look at $|m|$ versus well depth, the trends are apparent for each observed molecule; i.e., for a given observed molecule, the temperature dependence of the cross section changes with collision partner roughly according to the well-depth for the collision pair. In this paper, the size parameter r_0 (which we used in the geometric cross section πr_0^2) and the well depth parameter ϵ for the collision pair are those values that are obtained from the conformal intermolecular potentials (tabulated in Appendix 3 of Maitland et al.[24]) that have been determined from universal correlations of viscosity, diffusion coefficients, and thermal conductivities of gas mixtures. These are available for SF_6–X pairs but not for SeF_6–X or TeF_6–X. To complete the discussion of the general trends in the power m, we estimated $\epsilon(SeF_6\text{–X})$ and $\epsilon(TeF_6\text{–X})$ from $\epsilon(SF_6\text{–X})$ by a rational method. On the basis of the $\alpha_1\alpha_2$ factor in the dispersion part of the intermolecular potential we assume that the well depths are related approximately by $\epsilon(SeF_6\text{–X}) \approx (\alpha_{SeF_6}/\alpha_{SF_6})\epsilon(SF_6\text{–X})$. The ratio of electric dipole polarizabilities are 1.188 for SeF_6:SF_6 and 1.384 for TeF_6:SF_6.[33] These also lead to $\epsilon/k(SeF_6\text{–}SeF_6) \approx 293$ K and $\epsilon/k(TeF_6\text{–}TeF_6) \approx 398$ K, based on $\epsilon/k(SF_6\text{–}SF_6) = 207.7$ K. The average well-depth parameters for SeF_6 and TeF_6 with buffers, shown in Table IX, include these values. In Figure 6 we note that there is a clear trend of $|m|$ increasing with well depth, except that $^{15}N^{15}NO$ and $^{13}CO_2$ appear to have values that are somewhat low.

In their analysis of σ_J by semiclassical theory, Neilsen and Gordon[9] have found that contributions to the thermal average σ_J are J dependent. In the low-J states of the target molecule both strong and weak collisions contribute to the average, producing large σ-matrix elements that depend primarily on weak collisions dominated by the attractive potential. On the other hand, for high-J states of the target molecule, only strong collisions have

(35) Johnson, C. S.; Waugh, J. S. *J. Chem. Phys.* **1961**, *35*, 2020.
(36) Jameson, C. J.; Jameson, A. K. *J. Chem. Phys.* **1990**, *93*, 3237–3244.
(37) Trengove, R. D.; Robjohns, H. L.; Dunlop, P. J. *Ber. Bunsen-Ges. Phys. Chem.* **1984**, *88*, 450–453.
(38) Turfa, A. F.; Marcus, R. A. *J. Chem. Phys.* **1979**, *70*, 3035–3040.
(39) Kestin, J.; Ro, S. T. *Ber. Bunsen-Ges. Phys. Chem.* **1982**, *86*, 948–950.

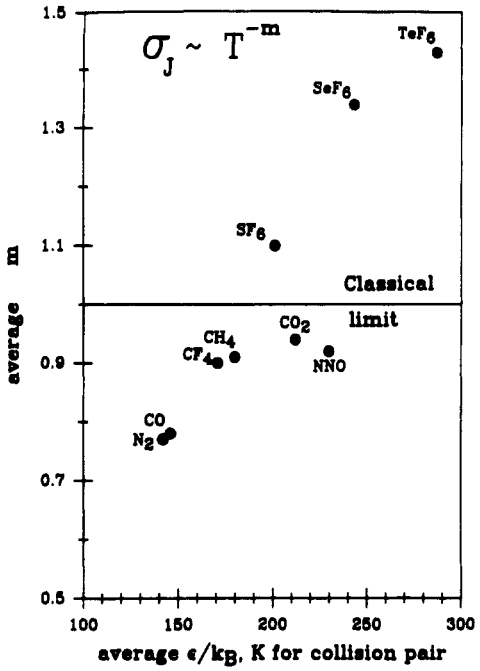

Figure 6. Average temperature dependence of the collision cross sections correlates with the average well depth.

sufficiently rapidly varying potentials to produce transitions, and thus the σ-matrix elements are smaller and depend primarily upon strong collisions dominated by the repulsive anisotropy. The overall temperature dependence described by $\sigma_J(T) = \sigma_J(300\,\mathrm{K})(T/300)^m$ then depicts the change in relative contributions of large and small σ-matrix elements as the relative weighting of these large-σ and small-σ elements change with temperature according to the populations of the rotational states and the initial rotational quantum numbers. The latter appear explicitly in the averaging since it is a spin–rotation interaction relaxation mechanism being observed. The correlation that we have found seems to indicate the importance of Gordon's large σ-matrix elements which depend primarily on the attractive potential. It is not surprising that the well depth has a significant influence on the averaging, but Figure 6 clearly shows that it is not simply a monotonic correlation. This is encouraging and can be taken as an indication that not just the well depth associated with the isotropic potential but the details of the anisotropy of the intermolecular potential are important in interpreting the temperature dependence of σ_J.

Contrary to previous expectation, there is important independent information to be gained about the anisotropy of the intermolecular potential from the temperature dependence of σ_J, which information would have been redundant and uninteresting if m values were all equal to the classical limit of -1. Furthermore, it is now possible to discern a correlation between the temperature dependence of the collision cross section and the average isotropic well depth.

Conclusions

We have measured the cross sections for changing the rotational angular momentum of SeF_6 and TeF_6 in collisions with self and with a set of 10 other molecules. The temperature dependence of these cross sections deviate significantly from the classically expected T^{-1} behavior. Prior to our work, there has been very little information on the temperature dependence of the collision cross sections for relaxation of the angular momentum vector. We compared the σ_J of SeF_6 and TeF_6 with the σ_J of other molecules previously studied in this laboratory. Although each collision pair has its unique temperature dependence and there is a sizeable range of such among the 10 collision partners, we have found a trend in the temperature dependence that ranges from a power predominantly less than to predominantly greater than this expected behavior. The deviation from the classically expected T^{-1} behavior is roughly in the order of increasing well depths:

$$N_2 = CO < CF_4 \lesssim CH_4 \lesssim NNO \lesssim CO_2 < SF_6 < SeF_6 < TeF_6$$

which is useful by itself for estimating rotational relaxation times and poses a theoretical challenge. With this study we have definitely established that, outside of experimental error, the temperature dependence of σ_J is generally different from T^{-1}, is uniquely different for each collision pair, and has a general trend in the order shown above for these linear molecules and spherical tops.

Acknowledgment. This research has been supported by The National Science Foundation (Grants CHE85-05725 and CHE89-01426). R.J.T. acknowledges the support of the Illinois Minority Graduate Incentive Program. Angel de Dios measured the ^{19}F chemical shifts of MoF_6 and WF_6 in the vapor phase relative to SiF_4.

Registry No. SeF_6, 7783-79-1; TeF_6, 7783-80-4; Ar, 7440-37-1; Kr, 7439-90-9; Xe, 7440-63-3; N_2, 7727-37-9; CO, 630-08-0; HCl, 7647-01-0; CO_2, 124-38-9; CH_4, 74-82-8; CF_4, 75-73-0; SF_6, 2551-62-4.

Matrix Infrared Spectra of the Products of the P_2 and O_3 Reaction

Matthew McCluskey and Lester Andrews*

Chemistry Department, University of Virginia, Charlottesville, Virginia 22901 *(Received: August 24, 1990)*

Molecular P_2 evaporated from heated GaP was codeposited with an argon/ozone stream at 12 K. Strong infrared product absorptions verify the spontaneous reaction of P_2 and O_3. Isotopic substitution, concentration variation, photolysis, and annealing behavior provide the basis for identification of primary reaction products PO and PO_2 and the new molecule P_2O and secondary products PO_3, P_2O_5, and cyclic P_4O_2. Photolysis produced further secondary reaction products oxo-bridged P_2O_4 and a new cyclic P_4O isomer, and annealing gave still another oxo-bridged P_2O_4 isomer. Infrared bands for these products are in good agreement with predictions from ab initio calculations.

Introduction

In recent years, considerable work has been done in this laboratory to study the oxidation reactions of phosphorus using matrix isolation infrared and optical spectroscopy. The aim of these studies has been to produce and characterize less common phosphorus oxides and to develop an understanding of the mechanisms of these very complicated reactions.[1-5] Most recently, a study of the reaction of P_2 and O_2 in argon matrices yielded

(1) Andrews, L.; Withnall, R. *J. Am. Chem. Soc.* **1988**, *110*, 5605. The band suggested for P_2O at 1197 cm^{-1} is probably due to a $(P_3)(PO)$ complex.
(2) Withnall, R.; Andrews, L. *J. Phys. Chem.* **1988**, *92*, 4610.

0022-3654/91/2095-2988$02.50/0